Acta Mechanica Solida Sinica (2023) 36:612–623
https://doi.org/10.1007/s10338-023-00408-w

# Topology Optimization of Acoustic–Mechanical Structures for Enhancing Sound Quality

**Lei Xu[1] · Weisheng Zhang[1] · Zhenyu Liu[2] · Xu Guo[1]**

Received: 28 February 2023 / Revised: 5 June 2023 / Accepted: 6 June 2023 / Published online: 11 July 2023


**Abstract**
Sound quality is one of the essential criteria for measuring the acoustic performance of acoustic devices. In contrast to the optimization of sound characteristics, both the quantitative description of sound quality and the numerical instability that may occur during optimization need to be investigated. In the present work, an explicit topology optimization approach is proposed to enhance the sound quality of acoustic–mechanical structures, where the sound quality is described, resorting to frequency response within a specified frequency band. To this end, the moving morphable component (MMC)-based approach is adopted to achieve the explicit topology design, and the mixed finite element method is introduced to evaluate the sound quality. With the use of the explicit description of MMC, the acoustic-structure boundary can be captured accurately, which is important for acoustic response analysis. Moreover, a regularization topology optimization formulation is also developed to avoid the numerical issues produced in some special frequency bands. Numerical examples demonstrate the effectiveness of the proposed approach in improving sound quality performance.

**Keywords** Acoustic-structure · Topology optimization · Moving morphable component (MMC) · Sound performance

## 1 Introduction

In recent decades, acoustic performance has been given wide concern in acoustic device design. For example, the speaker box is often expected to produce a uniform sound intensity distribution, headphones are required to have a frequency range close to that of human hearing, and electronic stethoscopes should reduce the response to outside noise. A state-of-the-art review of the recent progress in acoustic devices can be found in [1–4].

Compared with acoustic design in large equipment, the design in acoustic electronic devices is more complicated due to the specific design requirements within limited design space. Topology optimization, which aims to seek the optimal material distribution in a specified design domain with predefined constraints, has been applied to not only the design problems of mechanical structures but also the problems of structures under the multi-physics field in recent years, such as the proposed concerned acoustic–mechanical problems [5–7]. A large quantity of successful applications of topology optimization has been reported in [8–11] and the references cited therein. Unlike pure mechanical structural design, the acoustic field brings new issues for topology optimization, such as the difficulty in identifying the acoustic–mechanical interface between the structural and acoustic domains [12–14]. As the governing equations in the two physical fields are different, the segregated analysis method is often adopted for acoustic–mechanical problems, requiring a well-defined boundary between the acoustic and structural domains [15]. However, it is not a trivial task to satisfy this requirement in topology optimization. This is because the acoustic–mechanical interfaces can change dramatically during optimization. In this regard, combined with the re-meshing technique, the zero-level set in the level set method can implicitly identify the acoustic–mechanical boundary for minimizing the acoustic response inside the acoustic domain [16–18]. In order to maximize the first natural frequencies of the acoustic–mechanical model, Picelli et al. [19] realized that the element

✉ Weisheng Zhang
weishengzhang@dlut.edu.cn

✉ Xu Guo
guoxu@dlut.edu.cn

1 State Key Laboratory of Structural Analysis for Industrial Equipment, Department of Engineering Mechanics, International Research Center for Computational Mechanics, Dalian University of Technology, Dalian 116023, China

2 Changchun Institute of Optics, Fine Mechanics and Physics, Chinese Academy of Sciences, Changchun 130033, China

could switch between the acoustic domain and the structural domain by using the bidirectional evolutionary topology optimization (BESO) method. With the advantage of the discrete nature of the BESO method, the acoustic–mechanical boundary is defined and updated by discrete 0/1 design variables during the optimization process [20]. Yoon et al. [21] modified the material interpolation scheme and used the two-material rational approximation of material properties to delineate the distribution of acoustic and structural materials. Kook [22] used a redefined interpolation scheme with penalization in the extended BESO method and successfully solved the problem. Similar work also appeared in [23], which obtained smooth acoustic–mechanical boundaries by presenting floating projection topology optimization (FPTO) to push the design variables toward 0 or 1.

However, most studies on acoustic–mechanical problems focus on minimizing sound field characteristics, such as sound energy in an acoustic medium [24], sound pressure level (SPL) at a specified reference point/surface in an acoustic medium [25, 26], etc. There is little research on the optimization of sound quality characteristics of electronic devices. Actually, for electronic products that rely on acoustic performance, sound quality is one of the inescapable criteria. Sound quality refers to the sound from the machine/device that can reach the permissible values [27]. Generally, for sound quality optimization, it is expected that the SPL value is as high as possible but relatively stable in a certain frequency band. Obviously, this objective may cause some new issues. For example, numerical instability is caused by the competition among frequency points in the band, leading to non-convergence of the optimization results. Another issue is the computational effort problem. When the SPL optimization problem is solved by associating with the frequency band, the piecewise objectives may cause a large amount of unexpected computational cost. (The acoustic optimization problem is solved at each frequency point in the band.) Additionally, due to the existence of multifrequency points, the problem is more sensitivity to the acoustic–mechanical boundary, which means small boundary perturbations may cause large changes in the value of the objective function.

In this paper, the moving morphable component (MMC) approach [28] is adopted for the optimization of sound quality. The MMC method is a new topology optimization method that has been applied to various problems [29–33] due to its advantages such as explicit geometric description and fewer design variables. Similar approaches can also be found in [34–36]. For the acoustic problem concerned in the present work, the structural components in MMC are regarded as acoustic channels filled with acoustic media, and the parts outside the acoustic channels are defined as solid materials. Under this circumstance, the boundary between the acoustic domain and the structural domain can be well represented by the explicit geometric description of MMC. To address the issue of defining the material properties of an acoustic-structural cutting element in analysis, a mixed finite element formulation is applied, which realizes the transition between the acoustic domain and the structural domain. Furthermore, a parallel calculation program is introduced to improve calculation efficiency. Finally, a regularization formulation is proposed to improve the stability of the optimization problem.

The remainder of this article is organized as follows: Section 2 briefly discusses the problem of topology optimization on acoustic–mechanical structures under the MMC-based solution framework. Section 3 gives the numerical implementation issues in detail. In Sect. 4, some examples validate the effectiveness of the proposed method. Finally, some concluding remarks are presented in Sect. 5.

## 2 The Formulation for Acoustic–Mechanical Topology Optimization

In this section, the topology optimization formulation for the acoustic–mechanical interaction problem under the MMC-based framework is briefly introduced first. Generally, topology optimization for acoustic–mechanical problems aims to find the optimal material distribution of the acoustic medium in the prescribed design domain, allowing the device to achieve a certain acoustic performance (as shown in Fig. 1a). In the present work, our purpose is also to find a kind of acoustic medium distribution of effective acoustic channels (i.e., components in the MMC method) to improve sound quality. The final optimal channels can be generated through the movement, morphing, and overlapping of the components. The basic idea of the MMC-based acoustic–mechanical optimization problem is illustrated in Fig. 1b.

### 2.1 The Basic Idea of the MMC Method for Acoustic–Mechanical Topology Optimization

Under the MMC framework, the geometry and topology of an acoustic structure composed of channels can be expressed by the topology description function (TDF) [28] as follows:

$$\begin{cases} \phi(\boldsymbol{x}) > 0 \Leftrightarrow \boldsymbol{x} \in \Omega \\ \phi(\boldsymbol{x}) = 0 \Leftrightarrow \boldsymbol{x} \in \partial\Omega \\ \phi(\boldsymbol{x}) < 0 \Leftrightarrow \boldsymbol{x} \in D_a \backslash \Omega \end{cases} \tag{1}$$

where $D_a$ is the given design domain; $\Omega \subset D_a$ is the acoustic medium region, which should be composed of several channels, and $\phi(\boldsymbol{x})$ is the TDF of the entire acoustic space calculated with the use of $\phi = \max(\phi_1, \cdots, \phi_n)$. Actually, $\phi_i$ represents the TDF of the $i$th component, and can be expressed as

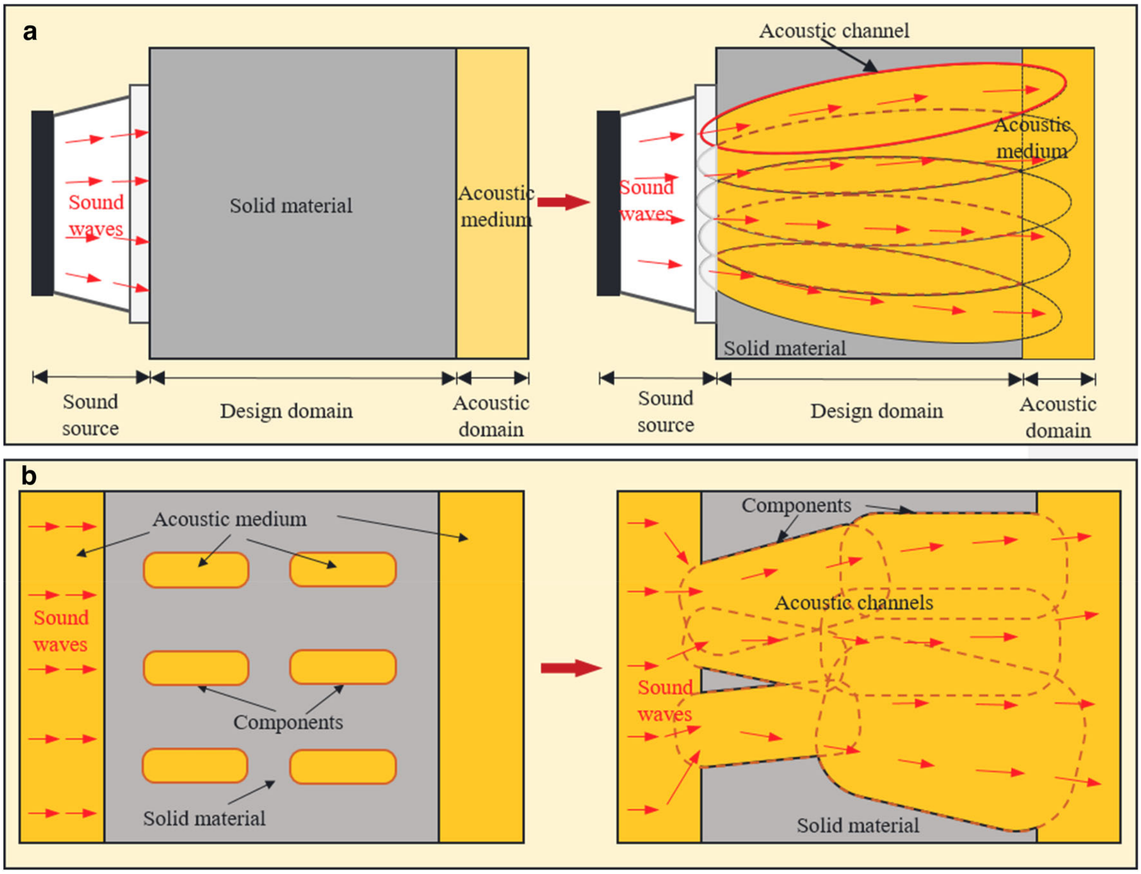


**Fig. 1** **a** The basic idea of topology optimization for acoustic–mechanical structures, **b** the basic idea of topology optimization for acoustic–mechanical structures via MMC

$$\phi_i(x, y, z) = 1 - \left(\frac{x'}{L_i^1}\right)^m - \left(\frac{y'}{h_1(x')}\right)^m - \left(\frac{z'}{h_2(x', y')}\right)^m \text{ (for 3D case)} \tag{2}$$

with

$$\begin{Bmatrix} x' \\ y' \\ z' \end{Bmatrix} = \boldsymbol{R} \begin{Bmatrix} x - x_{0i} \\ y - y_{0i} \\ z - z_{0i} \end{Bmatrix} \tag{3}$$

where $m$ is a large integer number ($m$=6 is used in the present work). Taking the 3D acoustic channel for example, $L_i^1$, $h_1\left(x'\right)$, and $h_2\left(x'\right)$ represent the half -lengths in the $x$-, $y$-, and $z$-directions of the $i$-th channel, respectively. Here, we set $h_1\left(x'\right) = L_i^2$, $h_2\left(x'\right) = L_i^3$, and $(x_{0i}, y_{0i}, z_{0i})$ as the coordinate of the center point of the $i$-th channel. $\boldsymbol{R}$ is the rotation transformation matrix calculated by

$$\boldsymbol{R} = \begin{bmatrix} \cos\beta_i \cos\theta_i & -\cos\beta_i \sin\theta_i & \sin\beta_i \\ \sin\alpha_i \sin\beta_i \cos\theta_i + \cos\alpha_i \sin\theta_i & -\sin\alpha_i \sin\beta_i \sin\theta_i + \cos\alpha_i \cos\theta_i & -\sin\alpha_i \cos\beta_i \\ -\cos\alpha_i \sin\beta_i \cos\theta_i + \sin\alpha_i \sin\theta_i & \cos\alpha_i \sin\beta_i \sin\theta_i + \sin\alpha_i \cos\theta_i & \cos\alpha_i \cos\beta_i \end{bmatrix} \tag{4}$$

where $\alpha_i$, $\beta_i$, and $\theta_i$ are the rotation angles of the $i$-th channel from the coordinate system $Oxyz$ to the coordinate system $O'x'y'z'$. Therefore, the design variable vector of the component (acoustic channel) (as shown in Fig. 2) can be expressed as

$$\boldsymbol{c} = \left(x_0, y_0, z_0, L^1, L^2, L^3, s_\alpha, s_\beta, s_\theta\right) \tag{5}$$

where $s_\alpha = \sin\alpha$, $s_\beta = \sin\beta$, $s_\theta = \sin\theta$.

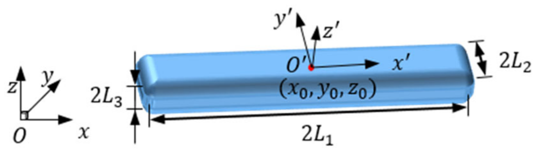


**Fig. 2** A three-dimensional acoustic channel (component)

Based on the above idea, the optimization problem can be expressed as follows:

$$
\begin{aligned}
&\text{Find}: \boldsymbol{c} = \left(\boldsymbol{c}_1^\top, \cdots, \boldsymbol{c}_n^\top\right)^\top \\
&\text{Minimize}: I = I(\boldsymbol{c}) \\
&\text{s.t.} \\
&\boldsymbol{K}(\boldsymbol{c})\boldsymbol{d} = \boldsymbol{f} \\
&V(\boldsymbol{c}) \le \overline{V} D_a \\
&\boldsymbol{c} \subset \mathcal{U}_{\boldsymbol{c}} \\
&\boldsymbol{d} = \overline{\boldsymbol{d}}, \ \text{on } \Gamma_{\boldsymbol{d}}
\end{aligned}
\tag{6}
$$

where $\boldsymbol{c}_i$, $i = 1, \cdots, n$ represents the design variable vector of the $i$-th component; $\mathcal{U}_{\boldsymbol{c}}$ is the admissible set allowed that $\boldsymbol{c}$ belongs to; $\boldsymbol{K}$ is the global stiffness matrix of the acoustic–mechanical problem; $\boldsymbol{d}$ is the structural response that includes mechanical and acoustic fields, respectively; $\boldsymbol{f}$ is the load vector; and $\overline{V}$ represents the volume fraction between 0 and 1.

### 2.2 Topology Optimization of Sound Quality Problem

For the traditional frequency point-based SPL maximization problem, the objective functional in Eq. (6) can be expressed as

$$I_1 = -\|p_i\|_2, \ \forall i \in [f_\mathrm{l}, f_\mathrm{u}] \tag{7}$$

where $p_i$ represents the frequency response obtained at frequency $i$ dropping in the frequency band $[f_\mathrm{l}, f_\mathrm{u}]$. It can be observed that $I_1$ intends to optimize a singular point. While in the sound quality optimization problem, the SPL response in the whole frequency band should be considered. Thus, the corresponding objective functional is written as

$$I_2 = \left\|p_i, p_j\right\|_2, \ \forall i, j \in [f_\mathrm{l}, f_\mathrm{u}] \tag{8}$$

where $\|p_i, p_j\|_2$ represents a kind of measure of the difference between $p_i$ and $p_j$. Actually, with the use of $I_2$, it can promote the values of the frequency response uniformly within the band $[f_\mathrm{l}, f_\mathrm{u}]$. However, it is still insufficient for sound quality optimization. Thus, the functional $I_2$ is further combined with $I_1$ as

$$I_3 = \eta I_2 + I_1 = \eta\|p_i, p_j\|_2 - \|p_k\|_2, \ \forall i, j, k \in [f_\mathrm{l}, f_\mathrm{u}] \tag{9}$$

where $\eta$ is a coefficient to control the magnitude of the uniformity of the frequency response in the band. Obviously, $I_3$ will uniformly adjust the values of frequency response and maximize them all simultaneously.

### 2.3 Regularized Formulation

As with the traditional frequency response optimization problem, when the concerned frequency is close to the resonant point, numerical instability may occur. In order to overcome this numerical issue, structural global mechanical performance criteria are often introduced into the optimization formulation to suppress numerical oscillations [39, 40]. In the present work, a similar idea is also adopted to regularize the solution space. Equation (6) with objective functional $I_3$ is further improved as

$$
\begin{aligned}
&\text{Find}: \boldsymbol{c} = \left(\boldsymbol{c}_1^\top, \ldots, \boldsymbol{c}_n^\top\right)^\top \\
&\text{Minimize}: I_3 = \eta\left\|p_i, p_j\right\|_2 - \|p_k\|_2 \\
&\text{s.t.} \\
&\boldsymbol{K}(\boldsymbol{c})\boldsymbol{d} = \boldsymbol{f} \\
&-\|p_t(\boldsymbol{c})\|_2 \le \bar{C} \\
&V(\boldsymbol{c}) \le \bar{V} D_a \\
&\boldsymbol{c} \subset \mathcal{U}_c \\
&\boldsymbol{d} = \overline{\boldsymbol{d}}, \ \text{on } \Gamma_d
\end{aligned}
\tag{10}
$$

where $p_t(\boldsymbol{c})$ is the frequency response at a fixed frequency, which should be indicated; and $\overline{C}$ is a predefined value. In this work, the frequency $t$ is the median of the concerned frequency band considered in the optimization problem.

## 3 Numerical Solution Aspects

### 3.1 Acoustic–Mechanical Finite Element and Material Interpolation Scheme

Ignoring the damping, the global stiffness matrix of the acoustic–mechanical structure coupling system in Eq. (6) can be expressed, with reference to [5], as

$$
\begin{bmatrix} \boldsymbol{K}_{uu} - \omega^2 \boldsymbol{M}_{uu} & -\boldsymbol{K}_{up} \\ -\rho_a \omega^2 \boldsymbol{K}_{up}^\top & \boldsymbol{K}_{pp} - \omega^2 \boldsymbol{M}_{pp} \end{bmatrix}
\begin{bmatrix} \boldsymbol{u} \\ \boldsymbol{p} \end{bmatrix}
=
\begin{bmatrix} \boldsymbol{f}_u \\ \boldsymbol{f}_p \end{bmatrix}
\tag{11}
$$

with

$$K_{uu} = \int_{\Omega_s} (\nabla N_s)^\top D_s \nabla N_s \mathrm{d}\Omega_s \tag{12}$$

$$M_{uu} = \rho_s \int_{\Omega_s} N_s^\top N_s \mathrm{d}\Omega_s \tag{13}$$

$$K_{up} = \int_{\Gamma_{sa}} N_s^\top n N_a \mathrm{d}\Gamma_{sa} \tag{14}$$

$$K_{pp} = \int_{\Omega_a} (\nabla N_a)^\top \nabla N_a \mathrm{d}\Omega_a \tag{15}$$

$$M_{pp} = \frac{1}{c_a^2} \int_{\Omega_a} N_a^\top N_a \mathrm{d}\Omega_a \tag{16}$$

where $\omega = 2\pi f$ is the angular frequency; $\rho_a$ and $\rho_s$ denote the material densities in the acoustic domain and structural domain, respectively; $\boldsymbol{K}_{uu}$ and $\boldsymbol{M}_{uu}$ are the structural stiffness matrix and mass matrix, respectively; $\boldsymbol{K}_{pp}$ and $\boldsymbol{M}_{pp}$ are the acoustic stiffness matrix and mass matrix, respectively; $\boldsymbol{K}_{up}$ is the coupling matrix; $\boldsymbol{u}$ is the displacement vector; $\boldsymbol{p}$ is the sound pressure vector; $\boldsymbol{f}_u$ is the load vector; $\boldsymbol{f}_p$ is the acoustic force vector; $\boldsymbol{N}_s$ and $\boldsymbol{N}_a$ are the shape functions for the structural domain and acoustic domain, respectively; $\boldsymbol{D}_s$ represents the constitutive matrix for isotropic material; $c_a$ is the speed of sound; and $\boldsymbol{n}$ is the normal vector on the coupled interface.

Therefore, the dynamic equilibrium equation of the acoustic–mechanical coupled system can be simplified as

$$\boldsymbol{K}\boldsymbol{d} = \boldsymbol{f} \tag{17}$$

with

$$\boldsymbol{K} = \begin{bmatrix} \boldsymbol{K}_{uu} - \omega^2 \boldsymbol{M}_{uu} & -\boldsymbol{K}_{up} \\ -\rho_a \omega^2 \boldsymbol{K}_{up}^\top & \boldsymbol{K}_{pp} - \omega^2 \boldsymbol{M}_{pp} \end{bmatrix} \tag{18}$$

$$\boldsymbol{d} = \begin{Bmatrix} \boldsymbol{u} \\ \boldsymbol{p} \end{Bmatrix} \tag{19}$$

$$\boldsymbol{f} = \begin{Bmatrix} \boldsymbol{f}_u \\ \boldsymbol{f}_p \end{Bmatrix} \tag{20}$$

With the use of the ersatz material model [41], the bulk modulus $\kappa^e$ and density $\rho^e$ associated with an element can be interpolated as

$$\kappa^e = \frac{(\kappa_1 - \kappa_2) \sum_{i=1}^{4} (H(\phi_i^e))^q}{4} + \kappa_2 \tag{21}$$

$$\rho^e = \frac{(\rho_1 - \rho_2) \sum_{i=1}^{4} (H(\phi_i^e))^q}{4} + \rho_2 \tag{22}$$

where $\kappa_1$ and $\rho_1$ are the bulk modulus and density of the acoustic material in the acoustic domain, respectively; $\kappa_2$ and $\rho_2$ are the bulk modulus and density of the structural material in the structural domain, respectively; and $\phi_i^e$, $i = 1, \cdots, 4$ are the values of the TDF associated with the four nodes of an acoustic element $e$. In this work, $q = 6$.

### 3.2 Approximation of the Maximum SPL Frequency Response

As discussed in the previous subsection, the objective functional $I_3$ serves two purposes. Obviously, it is impossible to achieve piecewise maximization at all points. Therefore, the piecewise response is replaced by the following maximum response in p-norm form,

$$I_3 = \eta \left\| p_i,\ p_j \right\|_2 - \| p_k \|_2 = \eta \left\| I_1^i,\ I_1^{\max} \right\|_2 - I_1^{\max} \tag{23}$$

with

$$I_1^{\max} = \left( \sum_{i=f_1}^{f_u} (I_1^i)^p \right)^{\frac{1}{p}} \tag{24}$$

where $p$ is a penalty factor ($p = 6$).

### 3.3 Sensitivity Analysis

By constructing the Lagrangian function, the objective functional $I_1$ in Eq. (7) is equivalent to

$$I^L = I_1 - \lambda_1 (\boldsymbol{K}\boldsymbol{d} - \boldsymbol{f}) - \lambda_2 \left( \bar{\boldsymbol{K}} \bar{\boldsymbol{d}} - \overline{\boldsymbol{f}} \right) \tag{25}$$

where $\lambda_1$ and $\lambda_2$ represent Lagrange multipliers. The derivative of $I^L$ regarding design variable $x$ is

$$\begin{aligned} \frac{\partial I^L}{\partial x} = \frac{\partial I_1}{\partial x} - \lambda_1 \left( \frac{\partial \boldsymbol{K}}{\partial x} \right) \boldsymbol{d} - \lambda_1 \boldsymbol{K} \left( \frac{\partial \boldsymbol{d}}{\partial x} \right) + \lambda_1 \frac{\partial \boldsymbol{f}}{\partial x} \\ - \lambda_2 \left( \frac{\partial \overline{\boldsymbol{K}}}{\partial x} \right) \overline{\boldsymbol{d}} - \lambda_2 \overline{\boldsymbol{K}} \left( \frac{\partial \overline{\boldsymbol{d}}}{\partial x} \right) + \lambda_2 \frac{\partial \overline{\boldsymbol{f}}}{\partial x} \end{aligned} \tag{26}$$

Suppose the load vector $\boldsymbol{f}$ is independent of the design variables $x$, we have $\frac{\partial \boldsymbol{f}}{\partial x} = 0$ and $\frac{\partial \overline{\boldsymbol{f}}}{\partial x} = 0$. Therefore, Eq. (26) can be simplified as

$$\frac{\partial I^L}{\partial x} = \frac{\partial I_1}{\partial x} - \lambda_1 \left( \frac{\partial \boldsymbol{K}}{\partial x} \right) \boldsymbol{d} - \lambda_1 K \left( \frac{\partial \boldsymbol{d}}{\partial x} \right) - \lambda_2 \left( \frac{\partial \overline{\boldsymbol{K}}}{\partial x} \right) \overline{\boldsymbol{d}} - \lambda_2 \overline{\boldsymbol{K}} \left( \frac{\partial \overline{\boldsymbol{d}}}{\partial x} \right) \tag{27}$$

The Lagrange multipliers $\lambda_1$ and $\lambda_2$ should satisfy the following boundary value problem

$$\lambda_1 \boldsymbol{K} \left( \frac{\partial \boldsymbol{d}}{\partial x} \right) + \lambda_2 \overline{\boldsymbol{K}} \left( \frac{\partial \overline{\boldsymbol{d}}}{\partial x} \right) = \frac{\partial I_1}{\partial x} \tag{28}$$

The derivative of $I_1$ regarding $x$ is

$$\frac{\partial I_1}{\partial x} = -\overline{\boldsymbol{d}}\frac{\partial \boldsymbol{d}}{\partial x} - \boldsymbol{d}\frac{\partial \overline{\boldsymbol{d}}}{\partial x} \tag{29}$$

Then, it yields

$$\lambda_1 \boldsymbol{K} = -\overline{\boldsymbol{d}} = \overline{\lambda_2 \overline{\boldsymbol{K}}} \tag{30}$$

$$\lambda_1 = \overline{\lambda_2} \tag{31}$$

Thus, Eq. (27) can be rewritten as

$$\frac{\partial I^L}{\partial x} = -2\mathrm{Re}\left(\lambda_1 \frac{\partial \boldsymbol{K}}{\partial x}\boldsymbol{d}\right) \tag{32}$$

where Re (.) represents the real part of a complex number.

When $I_3$ in $p$-norm form is concerned, the derivative of $I_3$ regarding $x$ is

$$\frac{\partial I_3}{\partial x} = 2\eta \sum_{i=f_1}^{f_u}\left(I_1^i - I_1^{\max}\right)\left(\frac{\partial I_1^i}{\partial x} - \frac{\partial I_1^{\max}}{\partial x}\right) - \frac{\partial I_1^{\max}}{\partial x} \tag{33}$$

with

$$\frac{\partial I_1^{\max}}{\partial x} = \left(\sum_{i=f_1}^{f_u}\left(I_1^i\right)^p\right)^{\frac{1}{p}-1} \sum_{i=f_1}^{f_u}\left(\left(I_1^i\right)^{p-1}\frac{\partial I_1^i}{\partial x}\right) \tag{34}$$

and

$$\frac{\partial I_1^i}{\partial x} = -2\mathrm{Re}\left(\lambda_1 \frac{\partial \boldsymbol{K}_i}{\partial x}\boldsymbol{d}_i\right), \forall i \in [f_1,\ f_u] \tag{35}$$

In Eq. (32), we have

$$\frac{\partial \boldsymbol{K}}{\partial x} = \begin{bmatrix} \frac{\partial \boldsymbol{K}_{uu}}{\partial x} - \omega^2 \frac{\partial \boldsymbol{M}_{uu}}{\partial x} & -\frac{\partial \boldsymbol{K}_{up}}{\partial x} \\ -\rho_a \omega^2 \frac{\partial \boldsymbol{K}_{up}^{\top}}{\partial x} & \frac{\partial \boldsymbol{K}_{pp}}{\partial x} - \omega^2 \frac{\partial \boldsymbol{M}_{pp}}{\partial x} \end{bmatrix} \tag{36}$$

Since the topology design variable $x$ only affects the acoustic elements, Eq. (36) can be simplified as

$$\frac{\partial \boldsymbol{K}}{\partial x} = \begin{bmatrix} 0 & 0 \\ 0 & \frac{\partial \boldsymbol{K}_{pp}}{\partial x} - \omega^2 \frac{\partial \boldsymbol{M}_{pp}}{\partial x} \end{bmatrix} \tag{37}$$

Under the MMC framework,

$$\frac{\partial \boldsymbol{K}_{pp}}{\partial x} - \omega^2 \frac{\partial \boldsymbol{M}_{pp}}{\partial x} = \frac{1}{4}\left(\sum_{e=1}^{\mathrm{NE}}\sum_{i=1}^{4} q\left(H\left(\phi_i^e\right)\right)^{q-1}\frac{\partial H\left(\phi_i^e\right)}{\partial x}\right)\left(\boldsymbol{K}_{pp}^e - \omega^2 \boldsymbol{M}_{pp}^e\right) \tag{38}$$

where $\boldsymbol{K}_{pp}^e$, $e = 1, \cdots$, NE and $\boldsymbol{M}_{pp}^e$, $e = 1, \cdots$, NE are the stiffness matrix and mass matrix of the acoustic element corresponding to $\phi_i^e = 1$, respectively. NE is the total number of acoustic elements in the acoustic design domain. The calculation of $\frac{\partial H(\phi_i^e)}{\partial x}$ can be found in [41].

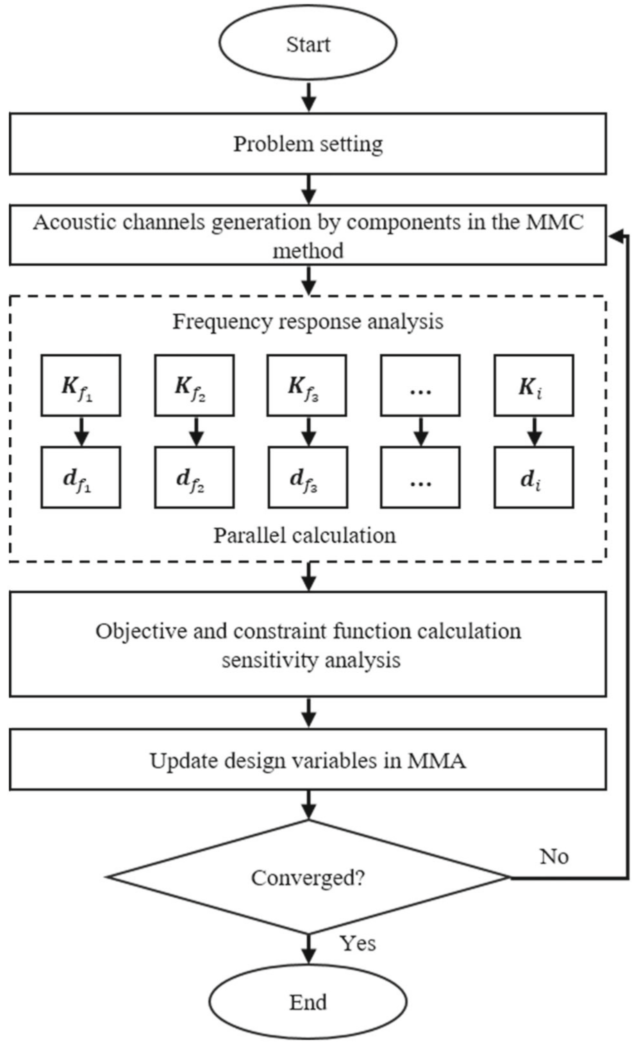


**Fig. 3** Topology optimization process of acoustic–mechanical structures under the proposed MMC framework

### 3.4 Parallel Algorithm

As mentioned in the previous sections, sound quality optimization is to optimize the SPL frequency response across the whole concerned frequency band. Therefore, the parallel computing technique is adopted to reduce computational efforts. In the present work, the Parallel Computing Toolbox integrated into the MATLAB software [42] is called to calculate both structural response and sensitivity analysis at each frequency point. Once the sensitivities are obtained, the method of moving asymptotes (MMA) [43] is adopted to evaluate and update the design variables. The topology optimization process of sound quality under the MMC framework is shown in Fig. 3.

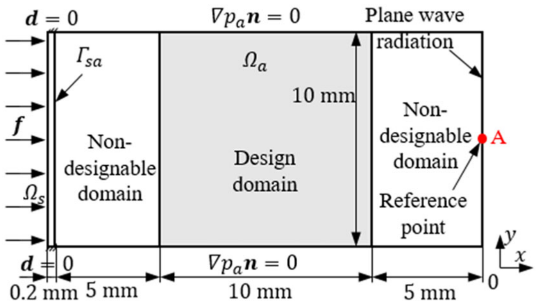


**Fig. 4** A 2D rectangular cavity structure

## 4 Numerical Examples

In this section, several examples are provided to demonstrate the effectiveness of the proposed method. Four-node square elements are used for the finite element discretization in 2D examples' examination. While in the 3D example, eight-node hexahedral elements and tetrahedral elements are adopted for discretizing the design domain and non-designable domain, respectively.

### 4.1 Loudness Optimization

First, a 2D rectangular cavity structure with loudness optimization at a single frequency point is solved for numerical performance testing purposes. As shown in Fig. 4, the domain of 20.2 mm × 10 mm is divided into the structural domain and the acoustic domain. The left part of the structural domain (0.2 mm × 10 mm) is filled with solid material, while the rest part of the acoustics domain (20 mm × 10 mm) is filled with acoustic material. A horizontal uniform load with a magnitude of $|\boldsymbol{f}| = 1$ N is applied to the structure. The upper and lower boundaries of the structural domain are defined as fixed boundaries, while the upper and lower boundaries of the acoustic domain are defined as sound hard boundaries. Plane-wave radiation is applied to the right boundary of the acoustic domain. The middle region filled with acoustic material is defined as the design domain (10 mm × 10 mm), where channels can be generated. Point A is selected as the reference point. Table 1 shows the parameters of the materials used in the problem. Acrylic plastic is selected as the solid material in the structural domain, while materials 1 and 2 in the acoustic domain are air and aluminum, respectively. The acoustic non-designable domain is filled with air. A uniform mesh of 202 × 100 is adopted for the whole structure discretization.

In this example, we intend to minimize the value of $I_1$ at a single frequency point referring to point A with a volume constraint. The concerned frequency in Eq. (6) is set to $f$=7000 Hz, and the volume fraction of the acoustic material $\overline{V}$ is set to 0.8. Figure 5a shows the initial distribution and final optimized design of the acoustic channels. Here, the components are made of material 1 representing the channels (air), and the rest region is made of material 2 (aluminum). In the final optimized design, two channels are generated. On the left side of the design domain, two small holes are first generated to receive sound. Then, the size of the channels becomes wider and wider from the left side to the right side to produce a trumpet shape. The shape can make the sound waves converge at reference point A and effectively increase the SPL. Figure 5b shows the iteration history of the objective function and the corresponding volume fraction constraint. It can be noted that the optimization process is relatively smooth, which is in favor of converging to the optimized value (at about step 180).

The comparison of SPL distribution between the original design and the optimized design is shown in Fig. 5c. Figure 5d shows the comparison of SPL curves for the original and optimized structures in the frequency range of 1000–10000 Hz. It can be observed that the SPL is increased to 106.33 dB from 102.89 dB at the concerned frequency point (i.e., $f$=7000 Hz).

### 4.2 Sound Quality Optimization

The same problem exhibited in Fig. 4 is resolved through sound quality optimization (i.e., $I_2$ and $I_3$). The concerned frequency band is set to 6000–8000 Hz, and the volume fraction $\overline{V}$ is set to 0.7. Five concerned frequency points are selected within this range (i.e., 6000 Hz, 6500 Hz, 7000 Hz,

**Table 1** Material parameters of structural domain and acoustic domain

| Material properties | Young's modulus (GPa) | Poisson's ratio | Density (kg/m$^3$) | Bulk modulus (GPa) |
|---|---|---|---|---|
| Structural domain (acrylic plastic) | 3.2 | 0.35 | 1190 | – |
| Acoustic domain material 1 (air) | – | – | 1.204 | $1.42 \times 10^{-4}$ |
| Acoustic domain material 2 (aluminum) | – | – | 2650 | 68.9 |

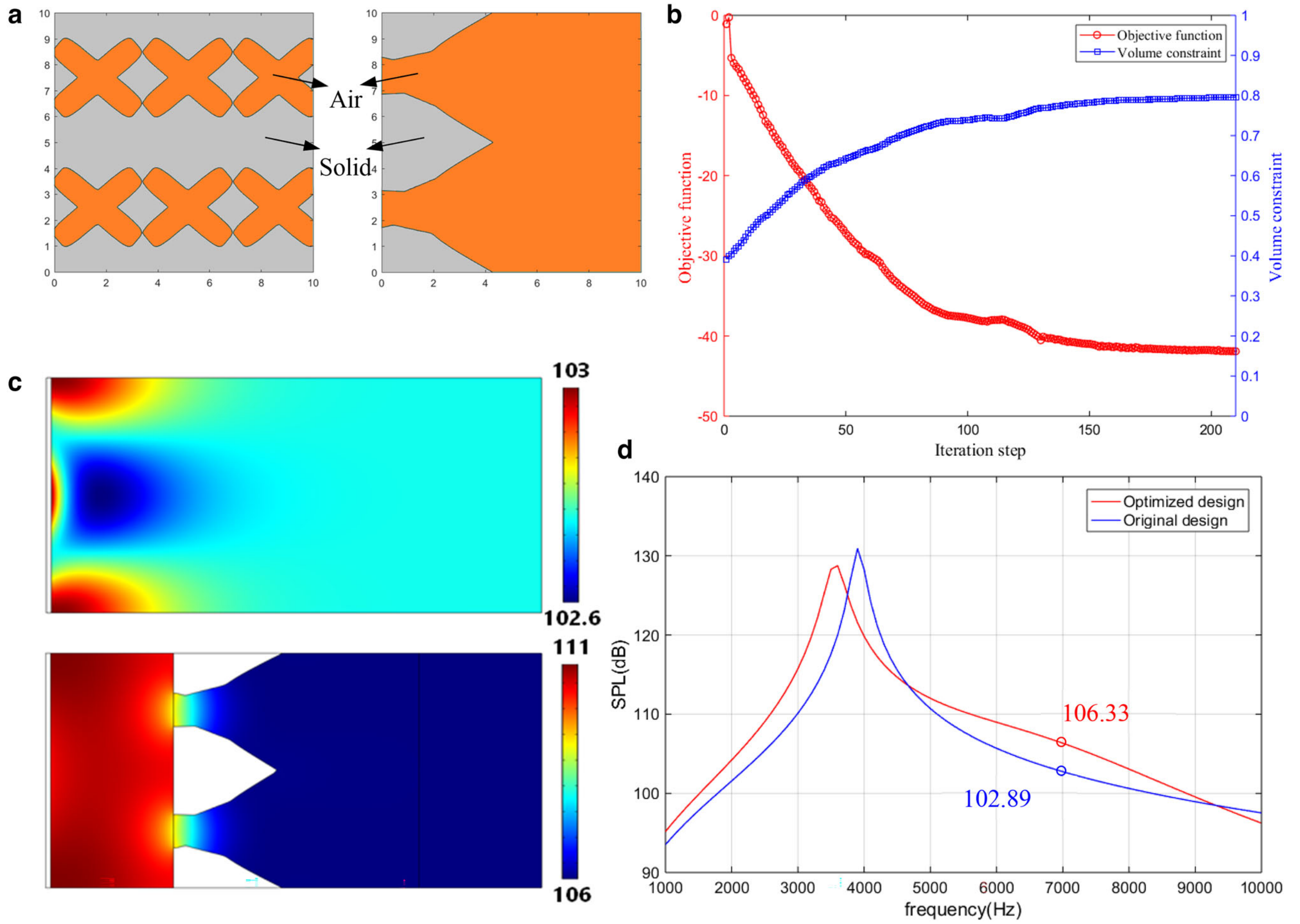


**Fig. 5** **a** The initial design and final optimized design of acoustic channels, **b** the iteration history of objective functional $I_1$ and volume constraint, **c** distribution of SPL (dB) of the 2D cavity structure at $f$=7000 Hz: original design (up) and optimized design (down), **d** SPL curves for original design and optimized design of the 2D cavity structure ([1000 Hz, 10,000 Hz])

7500 Hz, and 8000 Hz). If $I_2$ is used as the objective function, then the optimization will result in a design domain that is filled with pure solid material. Although this result can make the value of objective function $I_2$ optimal, it goes against our original optimization purpose.

Next, the objective function $I_3$ is adopted in the regularization formulation (i.e., Eq. (10)) with coefficient $\eta$=0.3 (a relatively large value of $\eta$ may impede the optimization of $I_1^{\max}$). The upper bound of the regularization constraint is set to $\overline{C}$=− 30.25 (case I) and $\overline{C}$=− 20.25 (case II) for comparison purposes. The optimization results of the two problems are given in Fig. 6a. In both results, two narrow channels can be observed clearly. However, with the decrease of $\overline{C}$, the two channels tend to merge and produce a horn shape (case I), which is more effective in improving the SPL to satisfy $-\|p_{7000}(\boldsymbol{c})\|_2 \leq \overline{C}$. Simultaneously, the values of SPL of all points in the band [6000 Hz, 8000 Hz] are increased in case I. While in case II, the width variation close to the left and right sides of the channels is not obvious. Although the capability of this kind of distribution in improving the maximum value of SPL is limited, it is more sensitive to decreasing the difference in the value of SPL between each pair of frequency points. Figure 6b shows the iteration history of the objective function and the constraint function. The SPL curves provided in Fig. 6c illustrate the above explanations. It can be observed from the curves that the maximum value of SPL of case I is increased to 114.03 dB from 105.69 dB (pure air design) at $f$=6000 Hz (107.10 dB in case II). Even at $f$=8000 Hz, the SPL is increased to 103.71 dB from 100.62 dB (100.28 dB in case II). However, the gap between the points ($f$=6000 Hz and $f$=8000 Hz) is 10.32 dB in case I (6.82 dB in case II).

## 4.3 Sound Quality Optimization of the 3D Cavity Structure

To further explore the numerical performance of the proposed approach, the sound quality optimization problem of

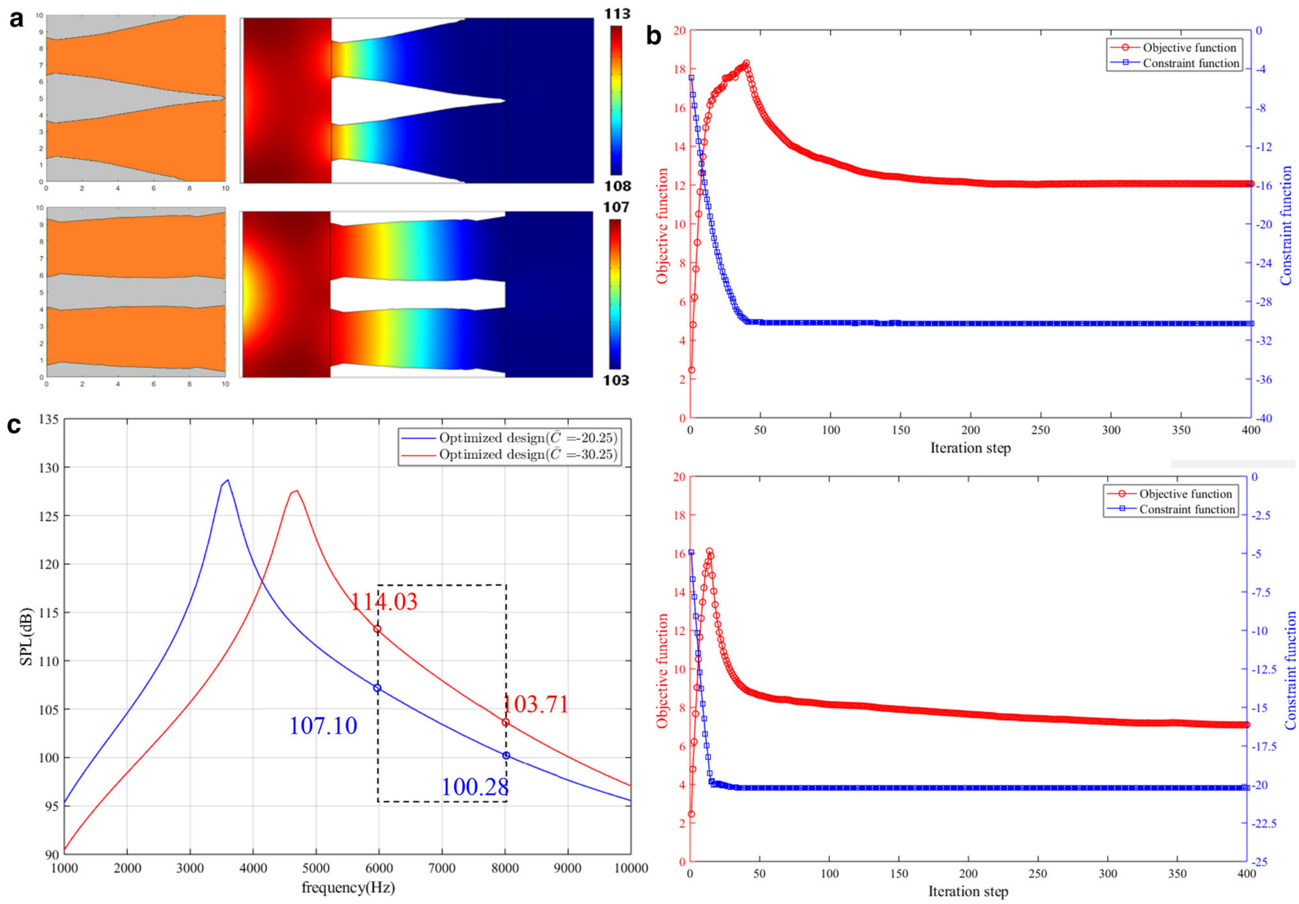


**Fig. 6** **a** The final optimized designs and the corresponding distributions of SPL (dB) of the 2D cavity structure: $\overline{C}$=− 30.25 (up) and $\overline{C}$=− 20.25 (down), **b** the iteration history of the objective function and the constraint function: $\overline{C}$=− 30.25 (up) and $\overline{C}$=− 20.25 (down), **c** the comparison of SPL curves of the 2D cavity structure ([1000 Hz, 10,000 Hz])

a 3D cavity structure is solved. Figure 7a shows the geometry of the cavity structure. The acoustic cavity structure is composed of a cavity and a vibrating plate with a size of 12 mm × 5 mm × 0.3 mm. The four surfaces (i.e., $s_1$, $s_2$, $s_3$, and $s_4$) of the plate are fixed. A uniformly distributed load is applied to the plate with a magnitude of $|\boldsymbol{f}|= 1$ N. The acoustic design domain is located at the upper part of the cavity structure with a size of 16 mm × 8 mm × 1.5 mm. The reference point A is positioned within the hemispherical acoustic field and is 25 mm away from the cavity. Spherical wave radiation is applied to surface $s_5$. Surface $s_6$ is the acoustic–mechanical coupling boundary. All the remaining acoustic boundaries are sound-hard. The same acoustic material used in the previous examples is adopted. To facilitate finite element calculation, the acoustic design domain uses regular hexahedral elements with a size of 0.25 mm, and the non-designable domain uses irregular tetrahedral elements. The corresponding mesh is displayed in Fig. 7b. This example intends to improve the sound quality in [7000 Hz, 10,000 Hz] using the optimization formulation of Eq. (10) with objective $I_3$ without regularization and a coefficient of $\eta = 0.17$.

Figure 8a shows the initial acoustic channels and the topology of the cavity structure, which are obtained by importing the optimized geometry into CAD software. It can be noted that the acoustic materials are distributed to form a slope plate, which effectively concentrates the sound waves from the sound source to the target reference point. Figure 8b shows the corresponding SPL distributions for the pure air design and the optimized design of the 3D cavity structure at 7000 Hz. The improvement of the sound quality can be observed from the SPL frequency response curve in Fig. 8c, where the SPL amplitudes at each frequency point are increased clearly (from 83.02 to 91.13 dB at 7000 Hz and from 78.34 to 82.54 dB at 10,000 Hz).

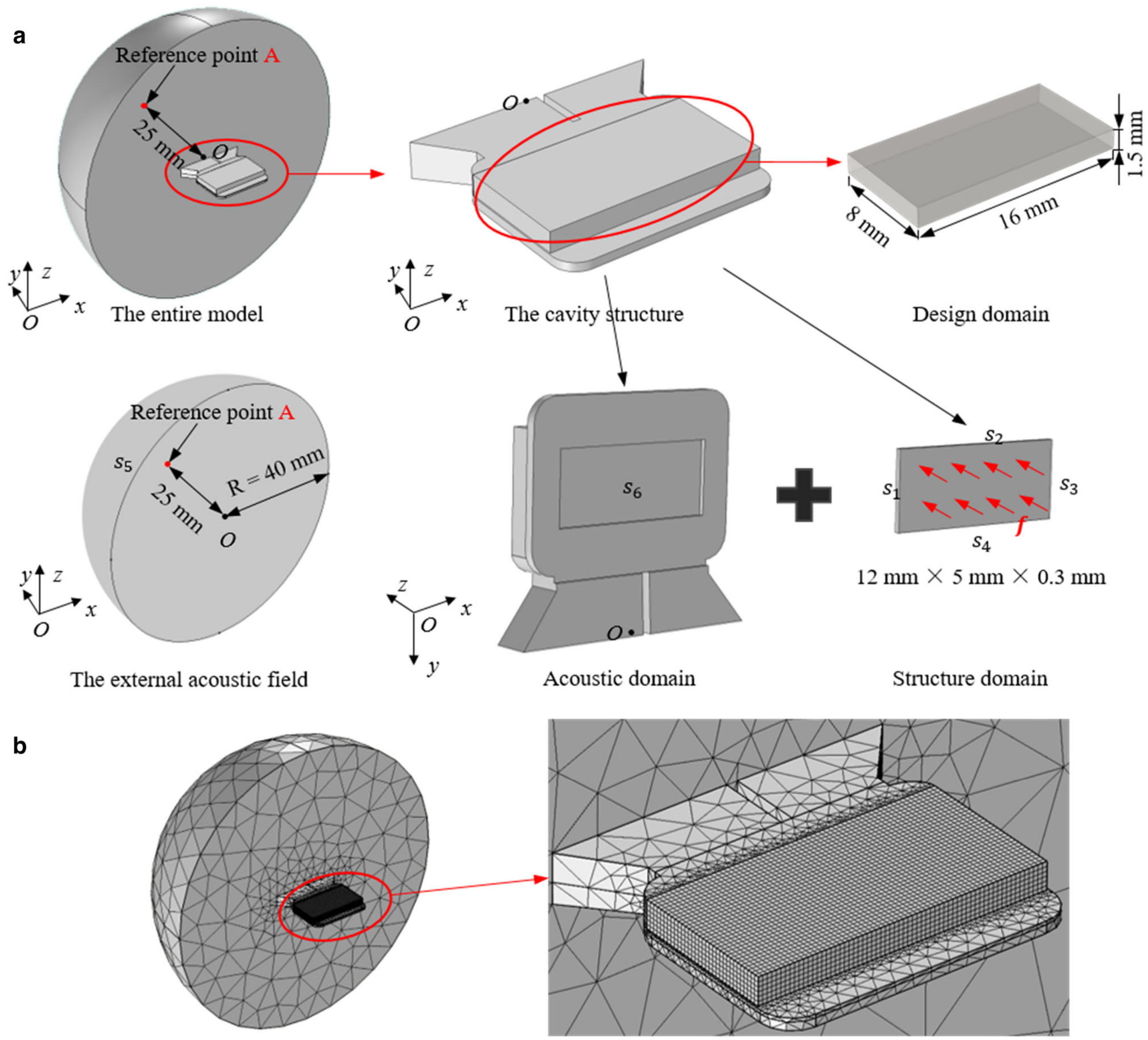


Fig. 7 **a** A 3D cavity structure, **b** finite element mesh of the entire model

## 5 Conclusion

In the present work, an explicit topology optimization method is proposed for improving the sound quality of acoustic cavities in acoustic–mechanical structures. Sound quality optimization is realized by optimizing the SPL of multiple frequencies simultaneously. A regularization formulation is also proposed to improve the numerical performance of the approach. Numerical examples show that sound quality optimization may impede the SPL increase in some cases. Therefore, the present optimization problem cannot be solved by only taking SPL maximization into consideration. The research results in this work are applicable to acoustic device design, such as speaker boxes, headphones, and electronic stethoscopes. However, only the frequency band of the examples is set in the high-frequency band. This is because multifrequency or full-frequency problems require a frequency sweep calculation, and the computational effort is relatively large. (The frequency points in the entire range should be seriously considered.) New solution techniques such as parallel techniques or data-driven computational methods need to be developed. In addition, the results obtained are only illustrated by numerical tests, which need to be supported by experimental measurements. We plan to carry out relevant research in this direction.

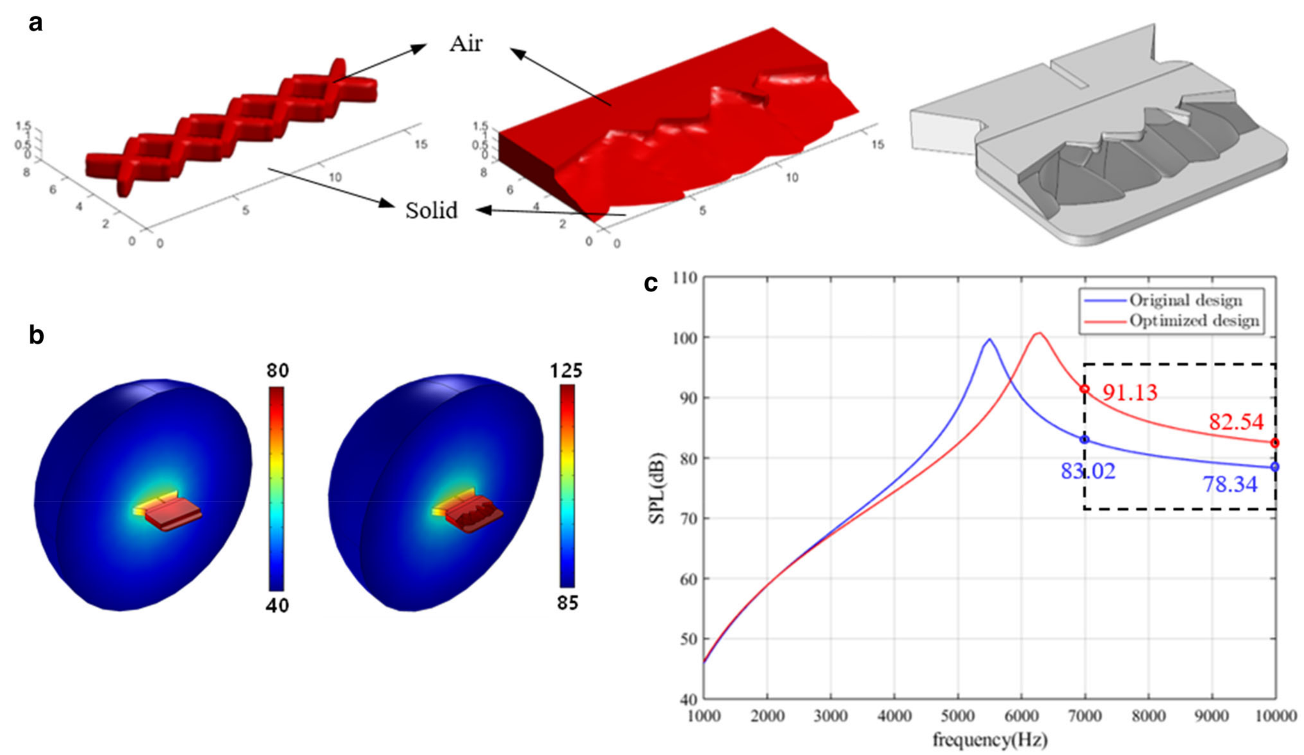


**Fig. 8** **a** The initial design of 3D acoustic channels and the optimized acoustic structure (components' plot and CAD plot), **b** distribution of SPL (dB) of the 3D cavity structure at $f$=7000 Hz: original design (left) and optimized design (right), **c** SPL curves of original design and optimized design of the 3D cavity structure ([1000 Hz, 10000 Hz])

**Author Contributions** WZ and XG designed the study; LX performed the research; ZL analyzed data; all authors contributed to the writing and revisions.

**Funding** The financial support from the Foundation for Innovative Research Groups of the National Natural Science Foundation (11821202), the National Natural Science Foundation (12272075), Liaoning Revitalization Talents Program (XLYC2001003, XLYC1907119), and Fundamental Research Funds for the Central Universities (DUT22QN238) are gratefully acknowledged.

**Availability of Data and Material** The data and material used or analyzed during the current study are available from the corresponding authors on reasonable request.

## Declarations

**Conflict of interest** The authors declare that they have no competing interests.

**Ethical Approval and Consent to Participate** This article does not contain any studies with human participants or animals performed by any of the authors.

**Consent for Publication** Consent for publication has been obtained from all individual participants included in the study.

## References

1. Kim HK, Jiang YW, Xu DP, Kwon JH, Hwang SM. Practical design of a speaker box with a passive vibrator (February 2018). IEEE Access. 2018;6:11443–51.
2. Barbieri R, Barbieri N. Acoustic horns optimization using finite elements and genetic algorithm. Appl Acoust. 2013;74(3):356–63.
3. Conlon TW, Nishisaki A, Singh Y, et al. Moving beyond the stethoscope: diagnostic point-of-care ultrasound in pediatric practice. Pediatrics. 2019;144(4):e20191402.
4. Ooi K, Xie Y, Lam B, Gan WS. Automation of binaural headphone audio calibration on an artificial head. MethodsX. 2021;8:101288.
5. Dilgen CB, Dilgen SB, Aage N, Jensen JS. Topology optimization of acoustic mechanical interaction problems: a comparative review. Struct Multidiscip Optim. 2019;60(2):779–801.
6. Zhao WC, Chen LL, Chen HB, Marburg S. Topology optimization of exterior acoustic–structure interaction systems using the coupled FEM–BEM method. Int J Numer Meth Eng. 2019;119(5):404–31.
7. Chen N, Yu DJ, Xia BZ, Liu J, Ma ZD. Microstructural topology optimization of structural-acoustic coupled systems for minimizing sound pressure level. Struct Multidiscip Optim. 2017;56(6):1259–70.
8. Xu ZX, Gao H, Ding YJ, Yang J, Liang B, Cheng JC. Topology-optimized omnidirectional broadband acoustic ventilation barrier. Phys Rev Appl. 2020;14(5):054016.
9. Fujii G, Takahashi M, Akimoto Y. Acoustic cloak designed by topology optimization for acoustic-elastic coupled systems. Appl Phys Lett. 2021;118(10):101102.

10. Ma L, Cheng L. Topological optimization of damping layout for minimized sound radiation of an acoustic black hole plate. J Sound Vib. 2019;458:349–64.
11. Kim KH, Yoon GH. Optimal rigid and porous material distributions for noise barrier by acoustic topology optimization. J Sound Vib. 2015;339:123–42.
12. Cerjan C, Kosloff D, Kosloff R, Reshef M. A nonreflecting boundary condition for discrete acoustic and elastic wave equations. Geophysics. 1985;50(4):705–8.
13. Mugnolo D. Abstract wave equations with acoustic boundary conditions. Math Nachr. 2006;279(3):299–318.
14. Boukhatem Y, Benabderrahmane B. Existence and decay of solutions for a viscoelastic wave equation with acoustic boundary conditions. Nonlinear Anal Theory Methods Appl. 2014;97:191–209.
15. Kook J, Jensen JS. Topology optimization of periodic microstructures for enhanced loss factor using acoustic–structure interaction. Int J Solids Struct. 2017;122:59–68.
16. Noguchi Y, Yamada T. Level set-based topology optimization for graded acoustic metasurfaces using two-scale homogenization. Finite Elem Anal Des. 2021;196:103606.
17. Shu L, Wang MY, Ma ZD. Level set based topology optimization of vibrating structures for coupled acoustic-structural dynamics. Comput Struct. 2014;132:34–42.
18. Desai J, Faure A, Michailidis G. Topology optimization in acoustics and elasto-acoustics via a level-set method. J Sound Vib. 2018;420:73–103.
19. Picelli R, Vicente WM, Pavanello R, Xie YM. Evolutionary topology optimization for natural frequency maximization problems considering acoustic–structure interaction. Finite Elem Anal Des. 2015;106:56–64.
20. Pedersen NL. Maximization of eigenvalues using topology optimization. Struct Multidiscip Optim. 2000;20(1):2–11.
21. Yoon GH, Jensen JS, Sigmund O. Topology optimization of acoustic–structure interaction problems using a mixed finite element formulation. Int J Numer Meth Eng. 2007;70(9):1049–75.
22. Kook J. Evolutionary topology optimization for acoustic–structure interaction problems using a mixed u/p formulation. Mech Based Des Struct Mach. 2019;47(3):356–74.
23. Hu J, Yao S, Huang XD. Topology optimization of dynamic acoustic–mechanical structures using the ersatz material model. Comput Methods Appl Mech Eng. 2020;372:113387.
24. Du JB, Olhoff N. Minimization of sound radiation from vibrating bi-material structures using topology optimization. Struct Multidiscip Optim. 2007;33(4):305–21.
25. Du JB, Olhoff N. Topological design of vibrating structures with respect to optimum sound pressure characteristics in a surrounding acoustic medium. Struct Multidiscip Optim. 2010;42(1):43–54.
26. Dühring MB, Jensen JS, Sigmund O. Acoustic design by topology optimization. J Sound Vib. 2008;317(3–5):557–75.
27. Letowski T. Sound quality assessment: concepts and criteria. Audio Engineering Society Convention 87. Audio Engineering Society; 1989.
28. Guo X, Zhang WS, Zhong WL. Doing topology optimization explicitly and geometrically—a new moving morphable components based framework. J Appl Mech. 2014. https://doi.org/10.1115/1.4027609.
29. Zhang WS, Li DD, Kang P, Guo X, Youn SK. Explicit topology optimization using IGA-based moving morphable void (MMV) approach. Comput Methods Appl Mech Eng. 2020;360:112685.
30. Zhang WS, Yan XY, Meng Y, Zhang CL, Youn SK, Guo X. Flexoelectric nanostructure design using explicit topology optimization. Comput Methods Appl Mech Eng. 2022;394:114943.
31. Sun JL, Tian Q, Hu HY, Pedersen NL. Topology optimization for eigenfrequencies of a rotating thin plate via moving morphable components. J Sound Vib. 2019;448:83–107.
32. Bai JT, Zuo WJ. Hollow structural design in topology optimization via moving morphable component method. Struct Multidiscip Optim. 2020;61(1):187–205.
33. Denimal E, Renson L, Wong C, Salles L. Topology optimization of friction under-platform dampers using moving morphable components and the efficient global optimization algorithm. Struct Multidiscip Optim. 2022;65(2):1–19.
34. Hoang VN, Nguyen NL, Nguyen-Xuan H. Topology optimization of coated structure using moving morphable sandwich bars. Struct Multidiscip Optim. 2020;61(2):491–506.
35. Nguyen HD, Hoang VN, Jang GW. Moving morphable patches for three-dimensional topology optimization with thickness control. Comput Methods Appl Mech Eng. 2020;368:113186.
36. Zhao YF, Hoang VN, Jang GW, Zuo WJ. Hollow structural topology optimization to improve manufacturability using three-dimensional moving morphable bars. Adv Eng Softw. 2021;152:102955.
37. Zhang SL, Gain AL, Norato JA. Adaptive mesh refinement for topology optimization with discrete geometric components. Comput Methods Appl Mech Eng. 2020;364:112930.
38. Smith H, Norato JA. Topology optimization with discrete geometric components made of composite materials. Comput Methods Appl Mech Eng. 2021;376:113582.
39. Ma ZD, Kikuchi N, Cheng HC. Topological design for vibrating structures. Comput Methods Appl Mech Eng. 1995;121(1–4):259–80.
40. Ma ZD, Kikuchi N, Hagiwara I. Structural topology and shape optimization for a frequency response problem. Comput Mech. 1993;13(3):157–74.
41. Zhang WS, Yuan J, Zhang J, Guo X. A new topology optimization approach based on moving morphable components (MMC) and the ersatz material model. Struct Multidiscip Optim. 2016;53(6):1243–60.
42. MATLAB. https://ww2.mathworks.cn/help/parallel-computing/parallel.pool.html.
43. Svanberg K. The method of moving asymptotes—a new method for structural optimization. Int J Numer Meth Eng. 1987;24(2):359–73.